J. Fluid Mech. (1997), *vol.* 332, *pp.* 1–21

Shear-induced lateral migration of Brownian rigid rods in parabolic channel flow

By LUDWIG C. NITSCHE[1] AND E. J. HINCH[2]

[1]Department of Chemical Engineering, The University of Illinois at Chicago, 810 South Clinton Street, Chicago, IL 60607, USA

[2]Department of Applied Mathematics and Theoretical Physics, The University of Cambridge, Silver Street, Cambridge CB3 9EW, UK

(Received 14 August 1995 and in revised form 17 July 1996)

This paper addresses the cross-stream migration of rigid rods undergoing diffusion and advection in parabolic flow between flat plates – a simple model of a polymer that possesses internal (rotational) degrees of freedom for which the probability distribution depends upon the local shear rate. Unequivocal results on the observable concentration profiles across the channel are obtained from a finite-difference solution of the full Fokker–Planck equation in the space of lateral position y and azimuthal angle ϕ, the polar angle θ being constrained to $\pi/2$ for simplicity. Steric confinement and hydrodynamic wall effects, operative within thin boundary layers, are neglected. These calculations indicate that rods should *migrate toward the walls*. For widely separated rotational and translational timescales asymptotic analysis gives effective transport coefficients for this migration. Based upon angular distributions at arbitrary rotational Péclet number – obtained here by a least-squares collocation method using trigonometric basis functions – accumulation at the walls is confirmed quantitatively by the effective transport coefficients. The results are extended to free rotation using spherical harmonics as the basis functions in the (ϕ, θ) orientation space. Finally, a critique is given of the traditional thermodynamic arguments for polymer migration as they would apply to purely rotational internal degrees of freedom.

1. Introduction

Except for deliberately contrived viscometric equipment, flows confined by walls are inhomogeneous in almost every natural or processing environment, i.e. they involve spatial gradients in shear. Dissolved polymers are observed to undergo cross-stream migration in inhomogeneous flow fields, thereby creating spatial gradients in rheological and other transport properties that can have important consequences in practical applications. In particular, slip flow has been explained by depleted layers at walls. The recent reviews by Jhon, Sekhon & Armstrong (1987), Larson (1992) and Agarwal, Dutta & Mashelkar (1994) discuss these aspects in relation to experimental investigations and to various theories that have been advanced for basic mechanistic understanding and more quantitative predictions.

The traditional mechanistic view is that polymers should tend to migrate toward regions of the flow where their conformational state is least restricted. Thus, shear deformation is expected to cause migration toward low shear, and steric confinement to cause migration away from walls (Bhave, Armstrong & Brown 1991). This paper

analyses the former effect. Except for the case of channels or pores of macromolecular dimensions, steric effects represent only a correction for the concentration field in a boundary layer, which we neglect here. (Of course, any resultant slip effects would have a global effect on the flow field.)

The above argument is most directly and appealingly phrased in thermodynamic terms, whereby polymers become less elongated and thus maximize their entropy by migrating toward low shear – e.g. toward the centreline in rectilinear tube flow. Calculations along these lines require an entropic potential written as a function of shear rate and/or other local properties of the flow (Marrucci 1972; Tirrell & Malone 1977; Cohen & Metzner 1982). In the elastic dumbbell model, the entropic opposition to uncoiling and stretching of many 'links' in a polymer chain is replaced with an enthalpic term: the potential energy of the spring (Marrucci 1972).

Thermodynamic reasoning cannot readily explain, however, why polymers migrate toward the concave side of curved streamlines, for which the prototypical experiment involves rotational Couette flow between concentric cylinders or cones (migration towards higher shear in the former case). A simple mechanical explanation hinges on misalignment between suspended dumbbells and the local streamlines, which can arise deterministically from Jeffery-orbit tumbling in the local shear field (Brunn 1983) or stochastically from Brownian motion. In this connection we cite relevant discussions in Sekhon, Armstrong & Jhon (1982), Brunn (1983) and Agarwal *et al.* (1994), which include the works of Shafer, Laiken & Zimm (1974), Bird (1979), Aubert & Tirrell (1980), and Aubert, Prager & Tirrell (1980). With very few exceptions (see e.g. Brunn & Chi 1984), most of the relevant kinetic theory, whether applied to rectilinear or curvilinear flows, has neglected the tumbling effect.

These are just two mechanistic pictures of polymer migration, which are mentioned here by way of illustrating that there is much discord – even as to the operative mechanism or direction of migration – between the various theories (Agarwal *et al.* 1994). A direct comparison between different approaches is muddled by the specific details of the polymer model in each case. There is an inherent paradox in the basic premise of stylized micromechanical theory that the macroscopic results should, in order to be valuable, transcend at least some of the details of the specific model used. What creates particular difficulty for bead–spring or bead–rod idealizations of polymers is that the approximations required to bring a particular theory of migration to fruition (e.g. neglect, truncation or preaveraging of bead-bead hydrodynamic interactions) can bear significantly on the final results. For rectilinear flows, kinetic theory predicts no lateral migration for a freely-draining dumbbell (Aubert & Tirrell 1980); but hydrodynamic interactions between the beads (or other sources of hydrodynamic anisotropy, such as concentration effects) do lead to lateral migration (Sekhon *et al.* 1982; Brunn & Chi 1984 and Brunn & Kaloni 1985). In fact, Brunn & Chi (1984) conclude from an unexpected *accumulation* at the walls that the more rigorous approach of *not* preaveraging hydrodynamic interactions must somehow be incorrect, because it disagrees with the accepted thermodynamic arguments. For further discussion of hydrodynamic interactions, see e.g. Larson (1992).

In view of the above observations, we conclude that there is significant value in attacking the question of cross-stream migration with a model microparticle that, if very simple, also allows definitive mathematical calculations based upon unassailable physical assumptions. It is in this spirit that we consider the shear-induced lateral migration of a Brownian rigid rod (equivalently, a suspension of non-interacting rods) in parabolic flow between flat plates (figure 1). Rigid rods represent, in their own right, a useful model of inextensible polymers. Further-

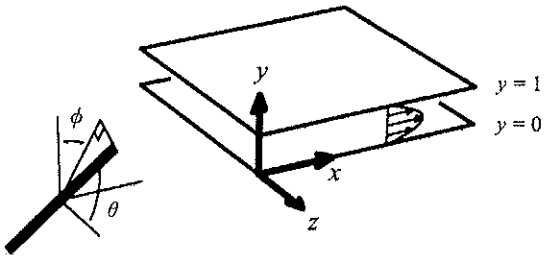

FIGURE 1. Diagram of the translational (x, y, z) and orientational (ϕ, θ) coordinates used to describe the motion of a rigid rod (prolate spheroid) between flat plates. Here the rod appears greatly exaggerated in size.

more, the shear-dependent distribution over rotational ('internal') degrees of freedom captures an essential physical analogy with more complex conformational degrees of freedom of flexible polymer chains. In the face of questions as to the lateral migration, we regard the Fokker–Planck equation and the resulting steady-state probability distribution in position-orientation space as the final arbiter. Fortunately, however, we are able to construct an asymptotic theory for the effective transport coefficients in a physical-space (i.e. purely translational) advection–diffusion equation, which predicts an accumulation *at the walls*, where the shear is highest and the rods are most strongly aligned against the randomizing influence of Brownian motion. This result being quite unexpected, we first offer some brief physical arguments before proceeding with the detailed theory.

From the perspective of kinetic theory the crucial element is position dependence of the orientation-average lateral diffusivity, which arises from anisotropic hydrodynamics. The lateral diffusivity decreases as one approaches the wall (higher shear rate) because the orientational distribution becomes biased toward orientations where motion across streamlines must overcome the higher broadside resistance coefficient. The rod is thrown out from the centreline by Brownian fluctuations more strongly than it is thrown back by the weaker fluctuations near the walls, so migration occurs toward the walls. (In Brownian dynamics simulations a similarly explained drift effect can arise; but in that case it is a physically spurious artifact of some algorithms, for which corrections must be made (Grassia, Hinch & Nitsche 1994).) Some previous investigations have addressed shear-dependent diffusivity of polymers – mostly in terms of its *modulating effect* upon migration. This aspect is reviewed by Agarwal *et al.* (1994), including the works of Prakash & Mashelkar (1991, 1992). But that shear-dependent diffusivity can directly *cause* lateral migration seems not to have been recognized before, except by Brunn & Kaloni (1985) and Brunn (1987) in regard to an encapsulated FENE dumbbell model.

In the studies of Brunn & Kaloni (1985) and Brunn (1987), hydrodynamic anisotropy and the crucial resultant conformational dependence of the (unrelated) friction and mobility tensors was attributed to concentration effects – i.e. partial confinement of each dumbbell within an effective 'reptation tube' due to its neighbours. Increased concentrations either near the wall or near the centre were predicted depending on the choice of parameters. They did not however calculate the migration velocity, and did not isolate the *physical* mechanism responsible for the migration. Their computation of the shear-dependent diffusivity invoked specific assumptions of preaveraging (which are avoided here with the rigid rod). Finally, in arriving at the conclusion that concentration should vary inversely with lateral diffusivity, these

papers seem to gloss over the order of taking derivatives in physical space *vs.* averages over conformations. This crucial interchange (multiplicative decomposition of phase-space probability density into bulk concentration *vs.* conformational structure) hinges on a wide separation between translational *vs.* internal timescales, which will here be treated systematically using two alternative perturbation arguments.

As we have mentioned above, our study ignores the steric hindrance near the walls. We also assume that the suspension is dilute so that the velocity profile remains Poiseuille flow. Recently Schiek & Shaqfeh (1995) have studied a semi-dilute suspension of slender rigid fibres flowing in a channel which is only a few fibres wide. They do include the steric hindrance and the change in the velocity profile, which is complicated by the non-local response of the semi-dilute suspension where the velocity varies over the length of a fibre. To make progress they make an expansion in small rotational Péclet number Pe and assume that the particle aspect ratio is infinite. We on the other hand study the case of arbitrary Péclet number and aspect ratio. In a sequel, Schiek & Shaqfeh (1997) have calculated the $O(Pe^2)$ correction which does show a shear-induced migration towards the wall. They compare their results with ours in their figure 6. The influence of walls has been considered further in two directions by Nitsche & Roy (1996), in the simpler case of a dilute suspension in homogeneous shear flow: (i) steric wall effects carried through Pe^4 terms for a point–bead dumbbell; (ii) combined hydrodynamic and steric wall effects carried through Pe^2 terms for dumbbells with appreciably sized beads. These inner behaviours are mentioned because they match smoothly with our simplified wall condition of vanishing normal derivative in physical space.

2. Fokker–Planck equation in position-orientation space

As a concrete example of lateral migration, we consider prolate spheroids undergoing translational and rotational Brownian motion while being carried along by a Poiseuille flow between two flat plates; see figure 1. With reference to the distance H between the plates, cross-sectionally averaged velocity $U/6$, and rotational diffusivity D_r, we define an overall rotational Péclet number $\mathscr{P} = U/(HD_r)$, which refers to the shear rate U/H at the wall. Written in dimensionless form, the advection–diffusion equation in position ($\boldsymbol{r}$) and orientation ($\boldsymbol{q}$) space for the probability density function $\tilde{P}(\boldsymbol{r}, \boldsymbol{q}, t)$ is as follows:

$$\frac{\partial \tilde{P}}{\partial t} + \nabla \cdot \left[\mathscr{P} y(1-y) e_x \tilde{P} - \epsilon \boldsymbol{D}(\boldsymbol{q}) \cdot \nabla \tilde{P}\right] + \nabla_{\boldsymbol{q}} \cdot \left[\mathscr{P}\gamma(y) \dot{\boldsymbol{q}}_s \tilde{P} - \nabla_{\boldsymbol{q}} \tilde{P}\right] = 0, \quad (2.1)$$

with $\dot{\boldsymbol{q}}_s$ the rotational velocity in a simple shear flow of unit strength in the absence of Brownian motion. Here

$$\epsilon = \left(D^{\parallel} + 2D^{\perp}\right) / \left(3D_r H^2\right), \quad (2.2)$$

where $D^{\parallel}$ and $D^{\perp}$ are the longitudinal and transverse translational diffusivities. Thus, $\epsilon = O(\ell^2/H^2)$, where ℓ denotes the size of the particles; see Rallison & Leal (1981). The reduced, orientation-dependent translational diffusivity $\boldsymbol{D}(\boldsymbol{q})$ will be written explicitly later. The quantity $\Gamma(y) = \mathscr{P}\gamma(y)$ plays the role of local rotational Péclet number, which varies linearly between the two walls,

$$\gamma(y) = 1 - 2y. \quad (2.3)$$

Note that $\Gamma(0) = -\Gamma(1) = \mathscr{P}$.

Integrating (2.1) over x and z gives an equation for the projected probability density function $P(y, \boldsymbol{q})$,

$$P(y, \boldsymbol{q}) = \int_{-\infty}^{\infty}\int_{-\infty}^{\infty} \tilde{P}(x, y, z, \boldsymbol{q})\,\mathrm{d}z\,\mathrm{d}x. \tag{2.4}$$

Thus we find

$$\frac{\partial P}{\partial t} - \epsilon D_{yy}(\boldsymbol{q})\frac{\partial^2 P}{\partial y^2} + \mathscr{L}\{\mathscr{P}\gamma(y)\}P = 0, \tag{2.5}$$

where we have used the shorthand notation

$$\mathscr{L}\{\Gamma\}P = \nabla_{\mathscr{Q}} \cdot [\Gamma \dot{\boldsymbol{q}}_s P - \nabla_{\mathscr{Q}} P]. \tag{2.6}$$

Physically most salient are (i) the absence of lateral advection and (ii) the orientational dependence of the lateral diffusivity. The probability density function is normalized,

$$\int_0^1 \int_{\mathscr{Q}} P(y, \boldsymbol{q})\,\mathrm{d}^n\boldsymbol{q}\,\mathrm{d}y = 1, \tag{2.7}$$

with n (= 1 or 2) the dimension of the orientation space. Avoiding considerations of steric confinement and hydrodynamic wall effects (Nitsche & Brenner 1990; Nitsche & Roy 1996; Schiek & Shaqfeh 1995, 1997), we simply stipulate no flux of particle *centres* through the boundaries $y = 0, 1$, irrespective of orientation $\boldsymbol{q}$ (Stasiak & Cohen 1983):

$$\frac{\partial P}{\partial y}(0, \boldsymbol{q}) = \frac{\partial P}{\partial y}(1, \boldsymbol{q}) = 0. \tag{2.8}$$

The resulting probability density function will err at a dimensionless distance of $O(\ell/H) = O(\epsilon^{1/2})$ from the walls. Equation (2.8) may be viewed as an *ad hoc* approximation, but it seems also to represent a leading-order asymptotic match to the rigorous inner solutions, at least to the order in Péclet number considered by Nitsche & Roy (1996).

The terms describing rotational advection and diffusion are now written explicitly in terms of the Euler angles θ and ϕ (figure 1),

$$q_x = \sin\theta\sin\phi, \quad q_y = \sin\theta\cos\phi, \quad q_z = \cos\theta. \tag{2.9}$$

We consider two cases:

Constrained. Axis vector $\boldsymbol{q}$ is confined to the (x, y)-plane. Rotation involves ϕ only, with $\theta = \pi/2$.

Free. Axis vector $\boldsymbol{q}$ can move over the whole unit sphere, involving both ϕ and θ. The rotational operator, (2.6), becomes

$$\mathscr{L}\{\Gamma\}P = \Gamma\frac{\partial}{\partial\phi}\left[\dot{\phi}_s(\phi)P\right] - \frac{\partial^2 P}{\partial\phi^2} \qquad \text{Constrained,} \tag{2.10}$$

$$= \Gamma\left\{\frac{\partial}{\partial\phi}\left[\dot{\phi}_s P\right] + \frac{1}{\sin\theta}\frac{\partial}{\partial\theta}\left[\dot{\theta}_s\sin\theta P\right]\right\}$$

$$- \frac{1}{\sin^2\theta}\frac{\partial^2 P}{\partial\phi^2} - \frac{1}{\sin\theta}\frac{\partial}{\partial\theta}\left[\sin\theta\frac{\partial P}{\partial\theta}\right] \qquad \text{Free.} \tag{2.11}$$

As given by Leal & Hinch (1971), the rotational advective velocities are

$$\dot{\phi}_s(\phi) = \tfrac{1}{2}\left[1 + \beta\cos(2\phi)\right], \tag{2.12}$$

$$\dot{\theta}_s(\phi, \theta) = \tfrac{1}{4}\beta\sin(2\phi)\sin(2\theta). \tag{2.13}$$

Axis ratio a/b	Rotation parameter β	Diffusive anisotropy α
10	0.98020	0.25588
20	0.99501	0.29818
50	0.99920	0.33748
100	0.99980	0.35854
∞	1.0	0.5

TABLE 1. Hydrodynamic coefficients for prolate spheroids (cf. Rallison & Leal 1981; Happel & Brenner 1983 §5–11).

The reduced translational diffusivity is

$$D_{yy}(\phi) = \left(1 + \tfrac{1}{4}\alpha\right) + \tfrac{3}{4}\alpha\cos(2\phi) \qquad \text{Constrained,} \tag{2.14}$$

$$D_{yy}(\phi,\theta) = 1 - \tfrac{1}{2}\alpha P_2(\cos\theta) + \tfrac{1}{4}\alpha P_2^2(\cos\theta)\cos(2\phi) \qquad \text{Free.} \tag{2.15}$$

Spherical harmonics are used in the latter case in anticipation of the numerical scheme to be used in §7. Values of the rotation parameter β and diffusive anisotropy α appear in table 1 for several axis ratios of a prolate spheroid. All calculations in this paper pertain to the axis ratio 100.

3. Direct numerical solution for the constrained case

In order to obtain the equilibrium probability density function $P(y,\phi;\epsilon)$, equations (2.5), (2.8) and (2.10) were solved by finite differences, using an evenly spaced discretization of 100 intervals in each direction for the position-orientation domain $0 \leqslant y \leqslant 1$, $0 \leqslant \phi \leqslant \pi$, and Euler stepping in time. Owing to the π-periodicity of the coefficients in (2.12) and (2.14), the angular interval $\pi < \phi < 2\pi$ is redundant. A conservative finite-difference formulation prevented numerical drift away from the overall normalization condition (2.7). Calculations were carried out at $\mathscr{P} = 10$ for seven values of the ratio of translational to rotational diffusivities: $\epsilon = 0.04, 0.02, 0.01, 0.005, 0.0025, 0.00125, 0.000625$. Each run started with a uniform initial distribution $P \equiv (2\pi)^{-1}$ and proceeded (stably) in time steps of $\delta t = 0.0001$ until the steady state was reached. For $\epsilon = 0.04$ it was sufficient to carry the time integration through to $t = 10$; each decrease in ϵ was accompanied by a proportional increase in the integration time to allow equilibration in y. The terminal time derivative at any node point did not exceed 3×10^{-9}. An angular integration (by evenly weighted 'rectangle rule', which is exponentially accurate for periodic, analytic functions) then gave the observable probability density (or concentration) profile across the flow channel:

$$\bar{P}(y;\epsilon) = 2\int_0^{\pi} P(y,\phi;\epsilon)\,\mathrm{d}\phi. \tag{3.1}$$

Examples of $P(y,\phi;\epsilon)$ and $\bar{P}(y;\epsilon)$ appear in figures 2 and 3, respectively.

In figure 2 the angular distribution $P(y,\phi;0.04)$ at fixed y is fairly uniform at the centreline ($y = 0.5$), where the shear rate vanishes, and becomes increasingly biased approaching the walls, exhibiting the expected central symmetry.

With reference to the singular limit $\epsilon \to 0$, we defer a derivation of the leading outer solution to §4, below, for which the first correction will be seen to appear at

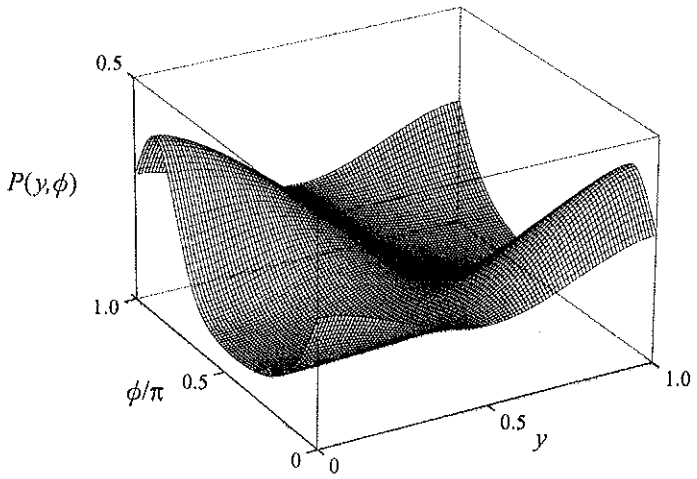

FIGURE 2. Steady-state probability density function $P(y, \phi)$ for constrained rotation of a prolate spheroid (axis ratio 100) with $\mathscr{P} = 10$ and $\epsilon = 0.04$.

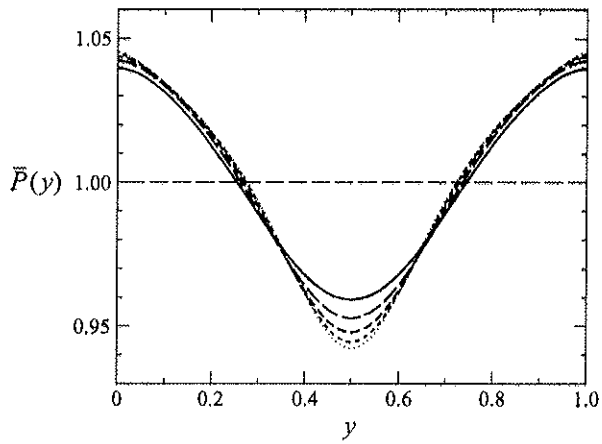

FIGURE 3. Steady-state angle-averaged probability density functions $\bar{P}(y)$ for $\mathscr{P} = 10$: ————, $\epsilon = 0.04$; — — , $\epsilon = 0.02$; — — — , $\epsilon = 0.01$; - - - - - , $\epsilon = 0.005$; ----------, $\epsilon = 0.0025$.

$O(\epsilon)$. Owing to the simplified boundary condition (2.8), the orientationally integrated lateral distribution $\bar{P}(y;\epsilon)$ must have zero slope at the sides. This is inconsistent with the requirement of a diffusive counterflux to balance the migration velocity, which is largest at the wall. Thus, we expect to find a boundary layer of $O(\epsilon^{1/2})$ characteristic thickness, whose role is to adjust the gradient. For example, in terms of the scaled lateral coordinate $\eta = (1 - y)\epsilon^{-1/2}$ near the wall $y = 1$ we have the inner problem,

$$D_{yy}(\boldsymbol{q})\frac{\partial^2 P}{\partial \eta^2} + \mathscr{L}\{\mathscr{P}\}P - \epsilon^{1/2}2\mathscr{P}\eta\nabla_{\mathscr{Q}} \cdot [\boldsymbol{q}_s P] = 0.$$

The leading outer solution (to be calculated in §4) is, in fact, uniformly valid – within terms of $O(\epsilon^{1/2})$ as dictated by the inner expansions.

Although the $O(\epsilon^{1/2})$ scaling of the boundary-layer thickness is difficult to ascertain directly from figure 3, we can confirm it indirectly using figure 4, which shows the

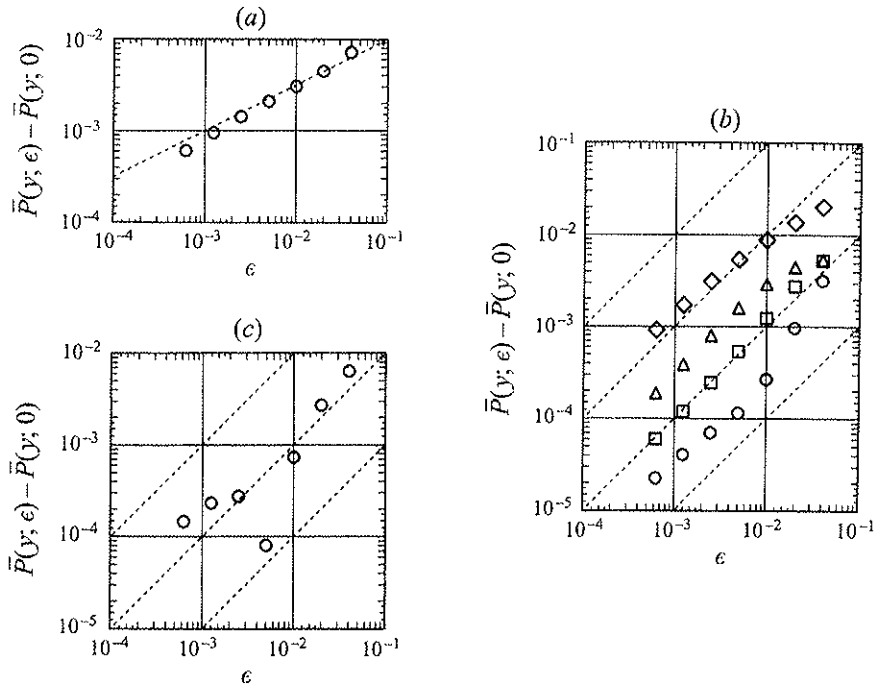

FIGURE 4. Extrapolation as $\epsilon \to 0$ of the numerical solution from §2 to the effective-coefficient theory from §4, for the case $\mathscr{P} = 10$: (*a*) $y = 0$; (*b*) ○, $y = 0.1$; □, $y = 0.2$; △, $y = 0.3$; ◇, $y = 0.5$; (*c*) $y = 0.4$.

numerical extrapolation of $\bar{P}(y;\epsilon)$ as $\epsilon \to 0$ for six fixed values of y. That corrections to the leading-order solution should scale like $\epsilon^{1/2}$ within the boundary layer is confirmed, at least approximately, from the extrapolation right at the wall ($y = 0$, figure 4*a*). One does observe some deviation from the expected slope 1/2; at the smallest values of ϵ this may be due to the fact that the boundary layers are no longer much thicker than the (fixed) step size. The ϵ scaling of the correction in the outer region is best exhibited at $y = 0.2, 0.3, 0.5$ in figure 4(*b*). At $y = 0.4$ (roughly where the curves for different values of ϵ fan out approaching the centreline in figure 3) the scaling at the larger values of ϵ plotted in figure 4(*c*) appears muddled. We also note that at $\epsilon = 0.04$ the boundary layers are not much thinner than the channel, so that at least some of our interior sampling points used to illustrate the outer extrapolation fail to start out lying 'safely' outside the boundary layers.

The profile $\bar{P}(y;\epsilon)$ levels off – by an $O(\epsilon^{1/2})$ amount within an $O(\epsilon^{1/2})$ distance from the wall – rather than continuing to increase approaching the wall. Thus there is $O(\epsilon)$ less accumulation of probability near the walls, which – by normalization – is balanced by $O(\epsilon)$ greater probability in between, in the outer region.

The above remarks are offered by way of checking the numerical solution against the expected scalings. Physically, however, it is of no particular importance to resolve the boundary layers at the walls, because both steric and hydrodynamic wall effects have been discarded at the outset.

4. Effective transport theory for the steady-state distribution

Away from the boundary layers, the singular limit $\epsilon \to 0$ represents a two-timescale problem, with fast rotational diffusion and slow translational diffusion (Rallison & Leal 1981). Before proceeding with such an analysis (§5), we shall first consider what is equivalent with regard to the *steady-state* version of (2.5): a regular perturbation expansion in ϵ, which is applicable away from the walls,

$$P(y,\boldsymbol{q};\epsilon) \;=\; P_0(y,\boldsymbol{q}) \;+\; \epsilon P_1(y,\boldsymbol{q}) \;+\; \ldots. \tag{4.1}$$

At zeroth order one finds

$$\mathscr{L}\{\mathscr{P}\gamma(y)\}P_0 \;=\; 0. \tag{4.2}$$

The most general solution is

$$P_0(y,\boldsymbol{q}) \;=\; g^e[\boldsymbol{q};\mathscr{P}\gamma(y)]c(y), \tag{4.3}$$

where $c(y)$ is the net concentration in physical space (corresponding to $\lim_{\epsilon\to 0}\bar{P}(y;\epsilon)$ in §3) and $g^e(\boldsymbol{q};\Gamma)$ represents the orientation structure (conditional probability given the concentration) as determined by the boundary-value problem

$$\mathscr{L}\{\Gamma\}g^e(\boldsymbol{q};\Gamma) \;=\; 0, \qquad \langle g^e(\boldsymbol{q};\Gamma)\rangle_{\mathscr{Q}} \overset{\text{def}}{=} \int_{\mathscr{Q}} g^e(\boldsymbol{q};\Gamma)\,\mathrm{d}^n\boldsymbol{q} \;=\; 1. \tag{4.4}$$

Here n denotes the dimension of the orientation space $\mathscr{Q}$: the cases $n = 1$ *vs.* $n = 2$ apply to constrained *vs.* free rotation, respectively. Averaged over the orientation space, the first-order equation is

$$\langle\mathscr{L}\{\mathscr{P}\gamma(y)\}P_1\rangle_{\mathscr{Q}} + \frac{\partial}{\partial y}\left\{\left[-\langle D_{yy}(\boldsymbol{q})g^e_\Gamma[\boldsymbol{q};\mathscr{P}\gamma(y)]\rangle_{\mathscr{Q}}\mathscr{P}\frac{\mathrm{d}\gamma}{\mathrm{d}y}\right]c(y) - \langle D_{yy}(\boldsymbol{q})g^e[\boldsymbol{q};\mathscr{P}\gamma(y)]\rangle_{\mathscr{Q}}\frac{\partial c}{\partial y}\right\} \;=\; 0, \tag{4.5}$$

where $g^e_\Gamma \overset{\text{def}}{=} \partial g^e/\partial\Gamma$. The first term vanishes by the divergence theorem, leaving a steady-state advection–diffusion equation written in the transverse coordinate y. One can then read off expressions for the effective migration velocity and diffusivity; these coefficients depend parametrically upon the local (Γ) and global ($\mathscr{P}$) rotational Péclet numbers:

$$\bar{D}^t(\Gamma) \;= \langle D_{yy}(\boldsymbol{q})g^e(\boldsymbol{q};\Gamma)\rangle_{\mathscr{Q}}, \tag{4.6}$$

$$\bar{V}(\Gamma,\mathscr{P}) = 2\mathscr{P}\langle D_{yy}(\boldsymbol{q})g^e_\Gamma(\boldsymbol{q};\Gamma)\rangle_{\mathscr{Q}} \;=\; 2\mathscr{P}\bar{V}_0(\Gamma), \tag{4.7}$$

with $\bar{V}_0$ a reduced migration velocity. (Note that $\bar{D}^t(\Gamma) > 0$ is an even function, whereas $\bar{V}_0(\Gamma)$ is an odd function that is positive when $\Gamma < 0$ (top half of the channel).) In terms of these quantities we define a local Péclet number for lateral migration, $2\mathscr{P}\bar{V}_0(\Gamma)/\bar{D}^t(\Gamma)$, which applies for $-\mathscr{P} \leqslant \Gamma \leqslant \mathscr{P}$.

The derivative with respect to Γ can be taken outside the integral over orientations in (4.7), whereupon $\bar{V}_0 = \mathrm{d}\bar{D}^t/\mathrm{d}\Gamma$. Using this fact upon integrating (4.5) one finds

$$\frac{\mathrm{d}\ln\{\bar{P}(y;\mathscr{P})\}}{\mathrm{d}y} = 2\mathscr{P}\frac{\bar{V}_0[\mathscr{P}(1-2y)]}{\bar{D}^t[\mathscr{P}(1-2y)]} \;=\; 2\mathscr{P}\frac{\mathrm{d}\{\ln\bar{D}[\mathscr{P}(1-2y)]\}}{\mathrm{d}[\mathscr{P}(1-2y)]} = -\frac{\mathrm{d}\{\ln\bar{D}[\mathscr{P}(1-2y)]\}}{\mathrm{d}y}, \tag{4.8}$$

whence

$$\bar{P}(y;\mathscr{P}) = \left\{\int_0^1 \frac{\mathrm{d}y'}{\bar{D}[\mathscr{P}(1-2y')]}\right\}^{-1} \frac{1}{\bar{D}[\mathscr{P}(1-2y)]}. \tag{4.9}$$

It is the multiplicative decomposition (4.3) – see also (5.6) below – that allows us to take the derivative with respect to Γ outside the orientational integral. This crucial step hinges on a wide separation between translational and internal timescales, and was glossed over by Brunn & Kaloni (1985) in arriving at the equivalent final result in connection with an encapsulated dumbbell model; see also Brunn (1987).

With regard to the integrand in (4.7) we note that differentiating (4.4) with respect to Γ gives an inhomogeneous differential equation for $g^e_\Gamma(\boldsymbol{q};\Gamma)$:

$$\mathscr{L}\{\Gamma\}g^e_\Gamma(\boldsymbol{q};\Gamma) = -\nabla_{\mathscr{Q}}\cdot[\mathscr{P}\dot{\boldsymbol{q}}_s\, g^e(\boldsymbol{q};\Gamma)], \qquad \langle g^e_\Gamma(\boldsymbol{q};\Gamma)\rangle_{\mathscr{Q}} = 0. \tag{4.10}$$

It is important to observe that lateral drift is a consequence of anisotropic mobility of the rod – in particular, the orientational dependence of the lateral diffusivity $D_{yy}(\boldsymbol{q})$. If D_{yy} were simply constant, then it could be moved outside the orientational integral in (4.7), and $\bar{V}_0$ would then vanish due to (4.10). In physical terms, slower lateral diffusion in more strongly aligned orientations leads to an accumulation of particles in such locations.

5. A two-timescale analysis

A separation of rotational *vs.* translational timescales was implicit in the regular perturbation scheme applied in §4 to the *steady-state* Fokker–Planck equation. This feature can be utilized explicitly in a two-timescale analysis of the parabolic equation (2.5); cf. Rallison & Leal (1981). Defining the fast (rotational) and slow (translational) time variables

$$\tau = t, \quad T = \epsilon t; \qquad \frac{\partial}{\partial t} = \frac{\partial}{\partial \tau} + \epsilon\frac{\partial}{\partial T}, \tag{5.1}$$

we write the two-scale expansion

$$P(y,\boldsymbol{q},t) = P_0(y,\boldsymbol{q},\tau,T) + \epsilon P_1(y,\boldsymbol{q},\tau,T) + \epsilon^2 P_2(y,\boldsymbol{q},\tau,T) + \ldots. \tag{5.2}$$

Substituting the above two formulas into the Fokker–Planck equation (2.5) gives the following hierarchy of equations:

$$\frac{\partial P_0}{\partial \tau} + \mathscr{L}\{\mathscr{P}\gamma(y)\}P_0 = 0, \tag{5.3}$$

$$\frac{\partial P_1}{\partial \tau} + \mathscr{L}\{\mathscr{P}\gamma(y)\}P_1 = -\frac{\partial P_0}{\partial T} + \frac{\partial}{\partial y}\left[D_{yy}(\boldsymbol{q})\frac{\partial P_0}{\partial y}\right], \qquad \text{etc.,} \tag{5.4}$$

together with the normalization conditions

$$\int_0^1 \langle P_0(y,\boldsymbol{q},\tau,T)\rangle_{\mathscr{Q}}\,\mathrm{d}y = 1, \quad \int_0^1 \langle P_i(y,\boldsymbol{q},\tau,T)\rangle_{\mathscr{Q}}\,\mathrm{d}y = 0 \quad (i \geqslant 1). \tag{5.5}$$

Now, the most general solution at zeroth order is

$$P_0(y,\boldsymbol{q},\tau,T) = c(y,T)g[\boldsymbol{q},\tau;\mathscr{P}\gamma(y)], \tag{5.6}$$

where the orientational distribution function $g(\boldsymbol{q},\tau;\Gamma)$ depends parametrically on the shear rate Γ as given by the orientation-space advection–diffusion equation

$$\frac{\partial g}{\partial \tau} + \mathscr{L}\{\Gamma\}g = 0, \qquad \langle g(\boldsymbol{q},\tau;\Gamma)\rangle_{\mathscr{Q}} = 1. \tag{5.7}$$

With this orientational normalization, $c(y, T)$ represents the observable (physical space) concentration. Inserting the form (5.6) into the first-order equation (5.4) and averaging over orientations gives

$$\frac{\partial}{\partial \tau}\langle P_1\rangle_{\mathscr{D}} = -\frac{\partial c}{\partial T} + \frac{\partial}{\partial y}\left\{\left\langle D_{yy}(\boldsymbol{q})\frac{\partial g}{\partial \Gamma}\right\rangle_{\mathscr{D}} \mathscr{P}\frac{\mathrm{d}\gamma}{\mathrm{d}y}\, c + \langle D_{yy}(\boldsymbol{q})g\rangle_{\mathscr{D}}\frac{\partial c}{\partial y}\right\}. \tag{5.8}$$

At long times compared to the rotational timescale we observe with reference to (4.4) and (4.10) that

$$g(\boldsymbol{q}, \tau; \mathscr{P}\gamma) \to g^e(\boldsymbol{q}; \mathscr{P}\gamma), \qquad \frac{\partial g}{\partial \Gamma}(\boldsymbol{q}, \tau; \mathscr{P}\gamma) \to g^e_\Gamma(\boldsymbol{q}; \mathscr{P}\gamma) \quad \text{as} \quad \tau \to \infty. \tag{5.9}$$

The secular behaviour we must avoid in (5.8) is linear growth in τ. Thus we must require that

$$\frac{\partial c}{\partial T} + \frac{\partial}{\partial y}\left\{\bar{V}_0[\mathscr{P}\gamma(y)]\left(-\mathscr{P}\frac{\mathrm{d}\gamma}{\mathrm{d}y}\right) c - \bar{D}^t[\mathscr{P}\gamma(y)]\frac{\partial c}{\partial y}\right\} = 0, \tag{5.10}$$

which is a Fokker–Planck equation written in lateral position y and the long (translational) timescale T using precisely the effective coefficients from (4.6) and (4.7).

6. Effective coefficients for constrained rotation

The periodic boundary-value problem (4.4) – with the operator $\mathscr{L}$ given by (2.10) – was solved by applying a least-squares collocation procedure to determine the coefficients of a truncated Fourier expansion,

$$g^e(\phi; \Gamma) \approx (2\pi)^{-1} + \sum_{m=1}^{M} [A_m(\Gamma)\cos(2m\phi) + B_m(\Gamma)\sin(2m\phi)]. \tag{6.1}$$

Restricted as indicated earlier to the interval $0 \leqslant \phi \leqslant \pi$, the differential equation was imposed at sufficiently many evenly spaced points,

$$\phi_i = \pi i/I, \qquad i = 1, \ldots, I, \tag{6.2}$$

to yield an overdetermined system of linear equations. The least-squares problem was solved with a LINPACK QR algorithm (Dongarra *et al.* 1979). Equal weighting of the equations at each of the collocation points corresponds to the (exponentially accurate) rectangle-rule integration of the error criterion

$$\mathscr{E} = \int_0^\pi \left[\mathscr{L}\{\Gamma\} g^e(\phi; \Gamma)\right]^2 \mathrm{d}\phi. \tag{6.3}$$

The approximate solution thus obtained was used to evaluate the right-hand side of (4.10) at the collocation points (6.2). Thereby, the same QR decomposition could be used to solve for the coefficients of $g^e_\Gamma(\phi; \Gamma)$,

$$g^e_\Gamma(\phi; \Gamma) \approx \sum_{m=1}^{M} [a_m(\Gamma)\cos(2m\phi) + b_m(\Gamma)\sin(2m\phi)]. \tag{6.4}$$

Only the back substitution had to carried out anew. Given the form (2.14) of the reduced translational diffusivity, the integrals (4.6) and (4.7) can be expressed in terms of the Fourier coefficients:

$$\bar{D}^t = 1 + \left(\tfrac{1}{4} + \tfrac{3}{4}\pi A_1\right)\alpha, \qquad \bar{V}_0 = \tfrac{3}{4}\pi a_1 \alpha. \tag{6.5}$$

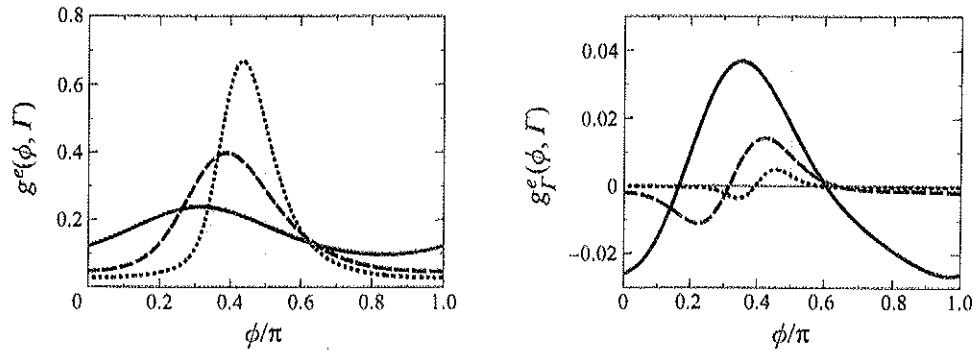

FIGURE 5. Equilibrium angular distributions $g^e(\phi;\Gamma)$ and $g^e_\Gamma(\phi;\Gamma)$ for constrained rotation at three values of the rotational Péclet number: ————, $\Gamma = 2$; — — —, $\Gamma = 10$; ----------, $\Gamma = 50$.

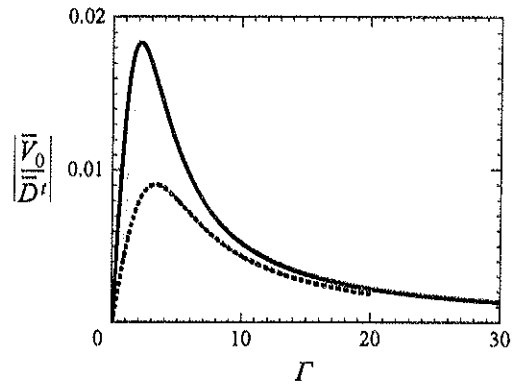

FIGURE 6. Reduced Péclet number for lateral migration $|\bar{V}_0/\bar{D}^t|$ plotted against rotational Péclet number Γ for constrained (————) *vs.* free (----------) rotation.

Examples of the equilibrium angular distribution functions $g^e(\phi;\Gamma)$ and $g^e_\Gamma(\phi;\Gamma)$ are illustrated in figure 5. These were computed with the Fourier series taken to $M = 12$, and with $I = 120$ collocation points. This discretization worked well up to $\Gamma = 50$; round-off errors in the QR calculation seemed to limit further increases in M (with $I = 10M$).

The reduced migration Péclet number $|\bar{V}_0/\bar{D}^t|$ is plotted against the local rotational Péclet number Γ in figure 6. With regard to the lateral migration velocity, the important part of the angular distribution $g^e_\Gamma(\phi;\Gamma)$ is the $\cos(2\phi)$ component, as is evident from (6.4) and (6.5). For small Γ the dominant mode is $\sin(2\phi)$; for large Γ the function $g^e_\Gamma(\phi;\Gamma)$ is uniformly small because the angular distribution $g^e(\phi;\Gamma)$ is so strongly aligned with the shear as to become relatively insensitive to further increases in Γ (figure 5; see Hinch & Leal 1972). This explains why the curve of reduced migration Péclet number $|\bar{V}_0/\bar{D}^t|$ *vs.* Γ undergoes a maximum in figure 6. The large-Γ end of the curve can be regarded as a regime of rotational 'saturation'. In figure 7 the local Péclet number for lateral migration $2\mathscr{P}\bar{V}_0/\bar{D}^t$ is plotted against y for various values of the overall rotational Péclet number $\mathscr{P}$. Angle-averaged probability distributions $\bar{P}(y;\mathscr{P})$, (4.9), are shown in figure 8; they exhibit accumulation at the walls. This effect requires orientational dependence of the translational diffusivity, (2.14), in order that variations in the degree of alignment across the channel can drive

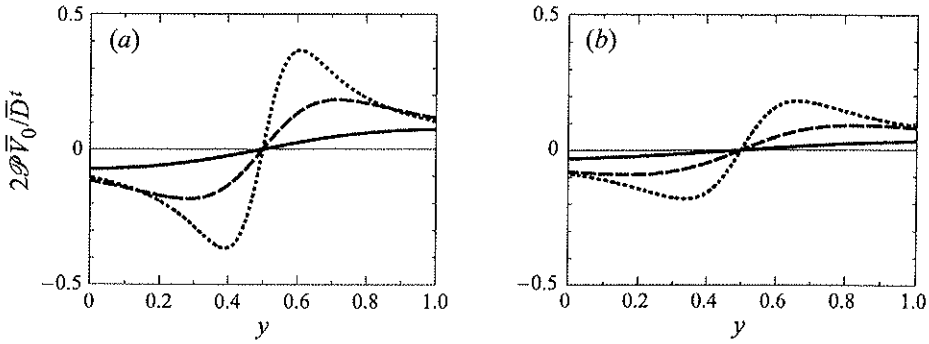

FIGURE 7. Local Péclet number for lateral migration $2\mathscr{P}\bar{V}_0/\bar{D}^t$ plotted against position y between the walls for three values of the overall rotational Péclet number: ————, $\mathscr{P} = 2$; — — —, $\mathscr{P} = 5$; ----------, $\mathscr{P} = 10$. (*a*) Constrained rotation. (*b*) Free rotation.

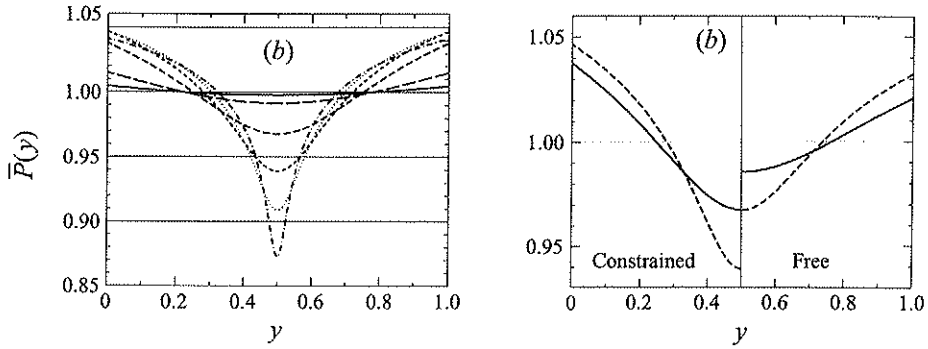

FIGURE 8. Orientation-averaged probability density function $\bar{P}(y;\mathscr{P})$ for various values of the overall rotational Péclet number $\mathscr{P}$. (*a*) Constrained rotation: ————, $\mathscr{P} = 1$; — — —, $\mathscr{P} = 2$; – – – – –, $\mathscr{P} = 5$; ----------, $\mathscr{P} = 5$; ....., $\mathscr{P} = 20$; ·····, $\mathscr{P} = 50$. (*b*) Comparison of constrained *vs.* free rotation ————, $\mathscr{P} = 5$; – – – – –, $\mathscr{P} = 10$.

lateral transport. As observed earlier, an orientation-independent diffusivity would give $\bar{V}_0 \equiv 0$.

At small values of the overall rotational Péclet number $\mathscr{P}$ (which coincides with the local rotational Péclet number Γ at the walls), alignment is weak throughout the channel, so $\bar{P}(y;\mathscr{P})$ is nearly uniform. For large $\mathscr{P}$, throughout most of the channel – except for an $O(\mathscr{P}^{-1})$ band about the centreline – the local rotational Péclet number Γ is large enough to lie within the saturation regime of figure 6. The degree of alignment with the shear is then uniformly high, which represents a small driving force for lateral migration. This type of behaviour is seen already at $\mathscr{P} = 10$ (figure 7), albeit in a mild form. Only near the centreline, where $|\bar{V}_0/\bar{D}^t|$ passes through its maximum as a function of Γ (figure 6), is lateral migration appreciable. Thus we see why the probability distributions $\bar{P}(y;\mathscr{P})$ in figure 8 first become more non-uniform as we increase $\mathscr{P}$, after which the central dip (internal boundary layer) becomes deeper and narrower, while the rest of the distribution becomes more uniform again.

7. Effective coefficients for free rotation

The solution of the boundary-value problem (4.4), (2.11) for free rotation, involving both ϕ and θ, was solved by an analogous least-squares collocation procedure, using spherical harmonics as the basis functions. Symmetry excludes odd orders and degrees; our orientational domain can be restricted to $0 \leqslant \phi \leqslant \pi$, $0 \leqslant \theta \leqslant \pi/2$. Thereby we use the following truncated expansion formula (Layec 1972):

$$g^e(\phi,\theta;\Gamma) \approx (4\pi)^{-1} + \sum_{n=1}^{N} A_n(\Gamma) P_{2n}(\cos\theta) + \sum_{n=1}^{N}\sum_{m=1}^{n} P_{2n}^{2m}(\cos\theta)\left[B_{n,m}(\Gamma)\cos(2m\phi) + C_{n,m}(\Gamma)\sin(2m\phi)\right], \quad (7.1)$$

$$g_\Gamma^e(\phi,\theta;\Gamma) \approx \sum_{n=1}^{N} a_n(\Gamma) P_{2n}(\cos\theta) + \sum_{n=1}^{N}\sum_{m=1}^{n} P_{2n}^{2m}(\cos\theta)\left[b_{n,m}(\Gamma)\cos(2m\phi) + c_{n,m}(\Gamma)\sin(2m\phi)\right]. \quad (7.2)$$

Using the least-squares collocation points

$$\phi_i = \pi i/I, \quad i = 1,\ldots,I; \qquad \theta_i = (\pi/2)j/J, \quad j = 1,\ldots,J, \quad (7.3)$$

each equation was weighted by the factor $(\sin\theta_j)^{1/2}$, to represent a discretized version (rectangle rule in ϕ, trapezoid rule in θ) of the integral error criterion

$$\mathscr{E} = \int_0^{\pi}\int_0^{\pi/2} \left[\mathscr{L}\{\Gamma\} g^e(\phi,\theta;\Gamma)\right]^2 \sin\theta \,\mathrm{d}\theta\,\mathrm{d}\phi. \quad (7.4)$$

With the same weighting, an analogous test calculation using *all* spherical harmonics (not just even orders and degrees) on the whole unit sphere recovered the correct symmetry to a high degree of accuracy. Using the decomposition (2.15), the transport-coefficient integrals (4.6) and (4.7) can be expressed as follows:

$$\bar{D}^t = 1 - \tfrac{2}{5}\pi\left(A_1 - 6B_{1,1}\right)\alpha, \qquad \bar{V}_0 = -\tfrac{2}{5}\pi\left(a_1 - 6b_{1,1}\right)\alpha. \quad (7.5)$$

Figure 9 shows examples of the orientational probability density functions $g^e(\phi,\theta;\Gamma)$ and $g_\Gamma^e(\phi,\theta;\Gamma)$ generated using $N = 8$, $I = 16$ and $J = 32$. This discretization worked well up to $\Gamma = 20$; as in §6, further increases in N, I and J seemed to be limited by round-off errors in the QR decomposition.

Stewart & Sorensen (1972) used Galerkin's method with spherical harmonics as the basis functions in order to solve (4.4) for the orientational distribution $g^e(\phi,\theta;\Gamma)$. Our scheme is applied to the further inhomogeneous equation (4.10) in which $g^e(\phi,\theta;\Gamma)$ appears on the right-hand side. Simplifications are possible for weak advective flows, using a regular perturbation expansion in the rotational Péclet number (Bird & Warner 1971; Layec 1972).

For the cases of constrained *vs.* free rotation, the respective functional dependencies of reduced migration Péclet number $|\bar{V}_0/\bar{D}^t|$ upon Γ are compared in figure 6. Figure 7(*b*) shows the local migration Péclet number $2\mathscr{P}\bar{V}_0/\bar{D}^t$ plotted against lateral position y. Finally, the actual probability density profiles are compared with the case of constrained rotation in figure 8(*b*). In both cases there is an accumulation at the walls, although the effect is weaker for free rotation. This is clearly not a purely entropic effect because it requires orientational dependence of the translational diffusivity,

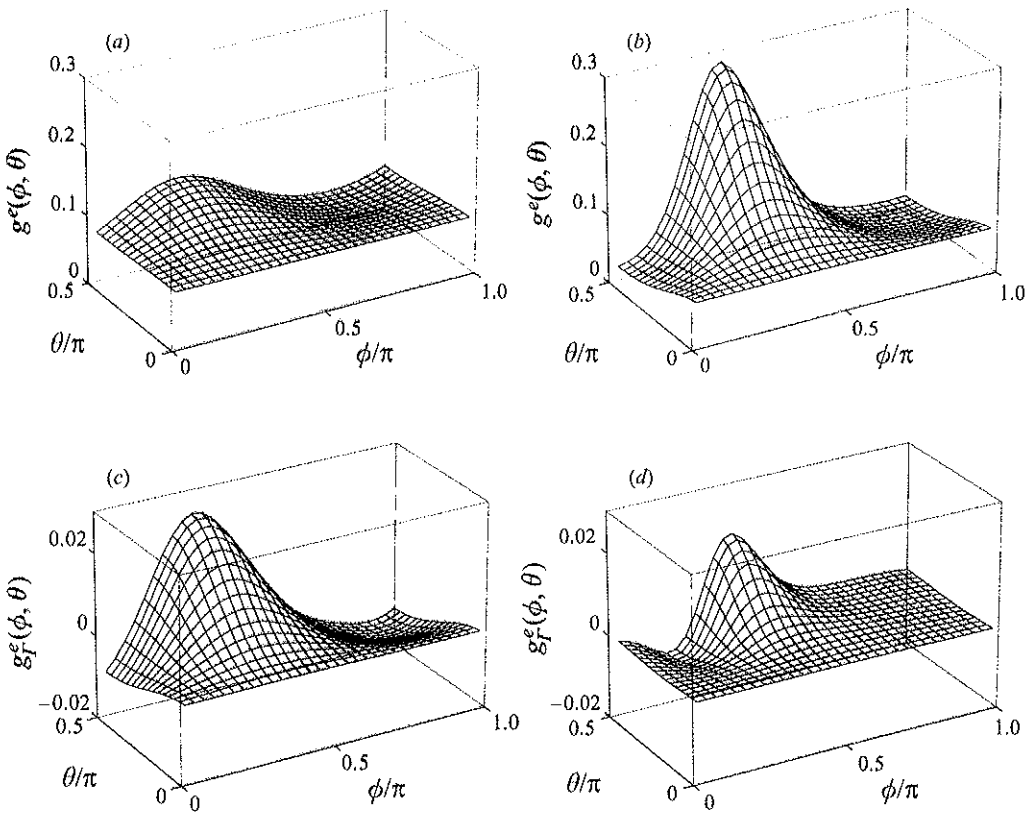

FIGURE 9. Equilibrium orientational distributions $g^e(\phi,\theta;\Gamma)$ and $g_\Gamma^e(\phi,\theta;\Gamma)$ for free rotation at two values of the rotational Péclet number Γ. (a,c) $\Gamma = 2$. (b,d) $\Gamma = 10$.

(2.14) and (2.15). As observed earlier, an orientation-independent diffusivity would give $\tilde{V}_0 = 0$.

8. Critique of the classical entropic argument

The classical thermodynamic argument for migration starts by noting that the particles are randomly oriented at the centreline and partially aligned near the walls in a channel flow. Now a suspension with aligned particles has a lower entropy, because entropy is maximized by a uniform distribution. Thus the orientationally averaged entropy is lower near the walls and higher on the centreline. It is then traditionally argued that the total entropy could be maximized if the concentration at the centre were to be increased by migration of the particles away from the walls. The basic premise that thermodynamics can resolve questions of migration must, however, immediately be viewed with suspicion when one considers the inherently non-conservative nature of the systematic orienting influence in the Brownian suspension. The viscous couples are not derivable from a potential energy, because vorticity in the flow makes the curl of the couple non-zero. Nevertheless, we shall proceed with a summary of various versions of the thermodynamic argument (as applied to our model problem of rigid rods) in order to illustrate its further pitfalls – all of which

arise, in one fashion or another, from the order in which integration over rotational degrees of freedom is combined with other operations.

Within a general configuration space $\mathscr{D}$, simple advection–diffusion of non-interacting objects in the presence of a potential V is described by the Fokker–Planck equation,

$$\frac{\partial P}{\partial t} = \nabla \cdot (P\boldsymbol{\omega} \cdot \nabla \mu), \tag{8.1}$$

with $\boldsymbol{\omega}$ the mobility tensor and μ the chemical potential per particle (within an arbitrary additive constant),

$$\mu = V + kT \ln P. \tag{8.2}$$

No-flux boundary conditions are applied on the walls:

$$\boldsymbol{n} \cdot (P\boldsymbol{\omega} \cdot \nabla \mu) = 0. \tag{8.3}$$

Their implementation in §2 regarded the walls only as hypothetical barriers to the penetration of particle *centres* (Stasiak & Cohen 1983), and neglected steric confinement as well as hydrodynamic wall effects.

The free energy density is

$$G = P\mu. \tag{8.4}$$

At equilibrium the total free energy is minimized, subject to normalization:

$$\dot{\mathscr{G}} = \frac{\mathrm{d}}{\mathrm{d}t} \int_{\mathscr{D}} G \, \mathrm{d}^n \boldsymbol{x} = -\int_{\mathscr{D}} P\boldsymbol{\omega} : (\nabla \mu)(\nabla \mu) \, \mathrm{d}^n \boldsymbol{x} = 0, \qquad \int_{\mathscr{D}} P \, \mathrm{d}^n \boldsymbol{x} = 1. \tag{8.5}$$

Positive-definiteness of $\boldsymbol{\omega}$ then requires the $-\nabla\mu$ driving force to vanish identically, which means μ must be constant throughout the configuration space. This is the usual statement of the equilibrium condition as applied to colloidal systems; see e.g. the discussions in Batchelor (1976, 1977) which refer to Einstein (1956). Thus in thermodynamic equilibrium one has the Maxwell–Boltzmann distribution

$$P \propto \mathrm{e}^{-V/kT}. \tag{8.6}$$

Written with reference to the full configuration space, this result is unequivocal whenever thermodynamics applies. But any projection down to a lower-dimensional subspace (e.g. averaging over internal degrees of freedom) becomes muddled by the question of the order of operations: should one project before or after minimizing $\mathscr{G}$?

8.1. *Orientational preaveraging*

In modelling polymer migration as the result of a shear-dependent entropic potential $\Upsilon(\Gamma)$, one implicitly preaverages over the conformational (and rotational) degrees of freedom, which are assumed to be in local equilibrium. A typical functional form based upon the elastic dumbbell model is as follows (Tirrell & Malone 1977; Cohen & Metzner 1982):

$$\Upsilon(\Gamma) = \tau^2\Gamma^2 - \tfrac{1}{2}\ln\left(1 + 2\tau^2\Gamma^2\right), \tag{8.7}$$

where τ represents a characteristic (dimensionless) macromolecular relaxation time. Marrucci (1972) gives a more complicated expression.

If we define the concentration $c(y)$ as the orientationally integrated probability

$$c(y) = \int_{\mathscr{Q}} P(y, \boldsymbol{q}) \, \mathrm{d}^n \boldsymbol{q}, \tag{8.8}$$

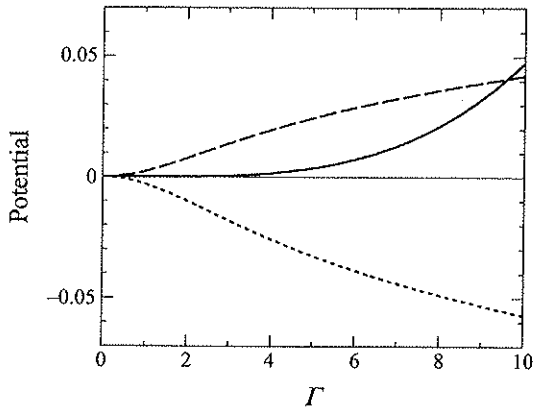

FIGURE 10. Entropic potential $\Upsilon(\Gamma)$ for $\tau = 0.05$, ————, compared with the orientational pseudo-potentials $\Psi(\Gamma)$, — — — , and $\tilde{\Psi}(\Gamma)/5$, ----------, for constrained rotation (§6). For the latter two functions, the respective reference energies (arbitrary additive constants) have been chosen to make the curves pass through the origin.

and the orientational structure function $g(y, \boldsymbol{q})$ as

$$g(y, \boldsymbol{q}) = P(y, \boldsymbol{q})/c(y), \tag{8.9}$$

then in the absence of any potentials, the orientationally integrated free energy density is

$$\bar{G}(y) = -kT \int_{\mathcal{Q}} P \ln P \, \mathrm{d}^n \boldsymbol{q} = -kTc \ln c - c\psi \tag{8.10}$$

where the effect of orientation g appears as a pseudo-potential energy,

$$\psi(y) = kT \int_{\mathcal{Q}} g(y, \boldsymbol{q}) \ln g(y, \boldsymbol{q}) \, \mathrm{d}^n \boldsymbol{q} \tag{8.11}$$

with

$$g(y, \boldsymbol{q}) = g^e[\boldsymbol{q}; \Gamma(y)], \tag{8.12}$$

as given in §§6 and 7 for the respective cases of constrained *vs.* free rotation. Thus ψ depends indirectly upon y through the local shear rate Γ: $\psi(y) = \Psi[\Gamma(y)]$. Figure 10 compares $\Psi(\Gamma)$ for constrained rotation with the entropic potential $\Upsilon(\Gamma)$ from (8.7), using the dimensionless relaxation time $\tau = 0.05$ for the latter.

Having *first* integrated over the rotational degree(s) of freedom to define a (projected) free energy density $\bar{G}$ that depends only upon position y, we now minimize the total free energy

$$\mathscr{G} = \int_0^1 \bar{G}(y) \, \mathrm{d}y \tag{8.13}$$

as a special one-dimensional case of the general equilibrium criterion (8.5), subject to a given constant number of particles:

$$\int_0^1 c(y) \, \mathrm{d}y = 1. \tag{8.14}$$

Thus one obtains the pseudo-Maxwell–Boltzmann distribution

$$c(y) = \mathrm{e}^{-\psi(y)/kT} \Big/ \int_0^1 \mathrm{e}^{-\psi(y)/kT} \, \mathrm{d}y. \tag{8.15}$$

This distribution has the greatest concentration on the centreline, where ψ is minimum. We wish to make several criticisms of the above argument; but first we must point out another possible answer which arises when the minimization of $\mathscr{G}$ is carried out *before* the orientational integration.

8.2. *Orientational postaveraging*

If we use the uniformity of chemical potential as the *starting point* for the integration over orientational degrees of freedom (having *first* minimized $\mathscr{G}$),

$$\bar{\mu}(y) = kT \int_{\mathscr{Q}} \ln P(y,\boldsymbol{q})\, \mathrm{d}^n\boldsymbol{q} = kT \ln c(y) + \tilde{\Psi}[\Gamma(y)] = \text{constant}, \tag{8.16}$$

then the resulting Maxwell–Boltzmann distribution – analogous to (8.15) – has a different orientational pseudo-potential,

$$\tilde{\Psi}(\Gamma) = \int_{\mathscr{Q}} \ln g^e(\boldsymbol{q};\Gamma)\, \mathrm{d}^n\boldsymbol{q}, \tag{8.17}$$

that actually *decreases* with increasing shear (figure 10). *Accumulation* at the walls would then be explained by asserting that confinement in orientation space must be compensated for by increased physical-space number density. This reasoning happens (only fortuitously) to be in qualitative agreement with the results from §§2, 6 and 7.

8.3. *Orientational potentials*

Suppose for this subsection that the orientation is not caused by the shear flow but by conservative couples, e.g. from a magnetic field, which are derivable from a potential energy $\Phi(\boldsymbol{q})$. Then

$$\dot{\boldsymbol{q}} = -\nabla_{\mathscr{Q}}\Phi \tag{8.18}$$

(with rotational mobility normalized to unity). In thermodynamic equilibrium, these couples create an orientation structure

$$\hat{g}^e(\boldsymbol{q}) = \mathrm{e}^{-\Phi(\boldsymbol{q})/kT} \Big/ \int_{\mathscr{Q}} \mathrm{e}^{-\Phi(\boldsymbol{q})/kT}\, \mathrm{d}^n\boldsymbol{q}. \tag{8.19}$$

If the strength of the conservative couples also varies in position, e.g. a non-uniform magnetic field, then the potential energy would also depend on position and orientation $\Phi(y,\boldsymbol{q})$. In thermodynamic equilibrium the probability distribution (8.6) would then take the form

$$P(y,\boldsymbol{q}) = \mathrm{e}^{-\Phi(y,\boldsymbol{q})/kT} \Big/ \int_{\mathscr{Q}} \int_0^1 \mathrm{e}^{-\Phi(y,\boldsymbol{q})/kT}\, \mathrm{d}y\mathrm{d}^n\boldsymbol{q}, \tag{8.20}$$

and so the concentration profile would be

$$c(y) = \int_{\mathscr{Q}} \mathrm{e}^{-\Phi(y,\boldsymbol{q})/kT}\, \mathrm{d}^n\boldsymbol{q} \Big/ \int_{\mathscr{Q}} \int_0^1 \mathrm{e}^{-\Phi(y,\boldsymbol{q})/kT}\, \mathrm{d}y\mathrm{d}^n\boldsymbol{q}. \tag{8.21}$$

Note that this distribution is different from that given by the classical thermodynamic argument for migration, (8.15), in which we substitute $\hat{g}^e(\boldsymbol{q})$ from (8.19) into the orientational potential formula (8.11). The error in the latter is that integration and exponentiation do not commute so that the exponential of the integrated energy $\mathrm{e}^{-\int \Phi}$ differs from the correct integral of the exponential of the energy $\int \mathrm{e}^{-\Phi}$. Hence we must view the classical thermodynamic argument with suspicion.

Now in the preceding paragraph, the variation with position of the strength of the couples led to a potential energy varying with position $\Phi(y, \boldsymbol{q})$, and this in turn led to the non-uniform concentration $c(y)$. Once the potential energy varies with position, there must be potential forces $-\partial\Phi/\partial y$ in addition to the potential couples $-\nabla_{\mathscr{Q}}\Phi$. Thus we can view the non-uniform concentration as a result of the non-zero forces acting *directly in physical space* on the particles. The shear flow is however different. It produces viscous couples whose strength varies with position but produces no viscous force. This is a further aspect of the non-conservative nature of the shear flow. Thus the shear flow lacks an important driving force for the migration of the particles. Further, it is clear that the classical argument uses ideas of thermodynamic equilibrium that are inapplicable when non-conservative forces and couples act.

8.4. *The driving force for lateral migration*

One problem with the classical thermodynamic argument summarized in §8.2 is that the orientationally integrated driving force

$$-\frac{\mathrm{d}\bar{\mu}}{\mathrm{d}y} = -\frac{\mathrm{d}}{\mathrm{d}y}kT\ln c - \frac{\mathrm{d}}{\mathrm{d}y}\int_{\mathscr{Q}} kT\ln g\,\mathrm{d}^n\boldsymbol{q} \tag{8.22}$$

does not generate the net migration flux. For each orientation, the force $\partial(kT\ln g)/\partial y$ must be multiplied by the probability P and the mobility D_{yy} – both of which depend on the orientation. The factor P would enter if the driving force were defined as the gradient of the orientationally integrated *free energy* $\mathrm{d}\bar{G}/\mathrm{d}y$, which is equivalent to the approach of §8.1. But the factor D_{yy} cannot find its way into any thermodynamic approach. The net flux is

$$-kT\left[\int_{\mathscr{Q}} D_{yy}(\boldsymbol{q})g(y,\boldsymbol{q})\,\mathrm{d}^n\boldsymbol{q}\right]\frac{\mathrm{d}c}{\mathrm{d}y} - kT\left[\int_{\mathscr{Q}} D_{yy}(\boldsymbol{q})\frac{\partial g}{\partial y}\,\mathrm{d}^n\boldsymbol{q}\right]c(y); \tag{8.23}$$

cf. (4.5). Thus again we see that the classical argument is in error by multiplying several averages, rather than first forming the product and then averaging.

Finally we recall our earlier remark that if the diffusivity is independent of the orientation, i.e. $D_{yy}(\boldsymbol{q})$ is constant, then the second integral vanishes in view of (4.10).

9. Concluding remarks

In this paper we have neglected both the steric and hydrodynamic hindrances which occur when the rods rotate near to the walls. Thus we cannot apply our results within a few rod lengths of the wall, as Brownian diffusion over such a length will be comparable to Brownian rotation. Schiek & Shaqfeh (1997) have studied the steric hindrance in a channel which is only a few rod lengths wide, making an expansion in small Péclet number Pe. They find a migration towards the wall, by the same mechanism. Their figure 5 shows that the shear-induced migration becomes independent of the gap width once the channel width H is wider than 15 rod lengths ℓ. In their figure 6 they compare their predictions for the shear-induced migration for $Pe = 0.5$, 2.0 and 5.0, $H/\ell = 35$ and $n\ell^3 = 0$ with our predictions in figure 8(*b*). They find reasonable agreement in the concentration profiles for $Pe = 0.5$ and $Pe = 2.0$. At $Pe = 5.0$ their $O(Pe^2)$ theory overpredicts our results, which is understandable because we find that the migration velocity has a maximum at $Pe \approx 3$.

For rigid Brownian rods, lateral migration hinges on the anisotropic mobility; otherwise spatial variations in the local degree of alignment cannot produce the crucial variations in orientation-average diffusivity by which the rods diffuse toward the walls

more vigorously than they are thrown back toward the centreline. When the characteristic timescales of translational *vs.* rotational diffusion are widely separated, the orientation structure at leading order is determined entirely by rotational equilibrium at the local shear rate, which leads to our prescription for computing the effective diffusivity and migration velocity. For rods of axis ratio 100, the end-on/broadside mobility ratio is approximately 1.66, whereby accumulation at the walls was limited to about 5% of the average concentration – this in the more conducive case of constrained rotations. When the axis ratio is taken to infinity, the mobility ratio is still only 2. Thus, substantially stronger migration will not be seen within the realm of purely rotational 'internal' degrees of freedom. These results for rigid rods are, however, sufficient to establish the basic mechanism of cross-stream migration – and to point out its inherent inaccessibility to entropic arguments – while avoiding the assumptions and approximations that would muddle or perhaps even obscure the analogous theory for more complicated bodies with conformational degrees of freedom. With reference to the shear-dependent diffusivity of elastic-dumbbell models of polymers (Brunn & Kaloni 1985; Brunn 1987; Öttinger 1987, 1989*a*,*b*; Prakash & Mashelkar 1991, 1992) it would be interesting to consider the effect of the increased 'frictional grip' of the fluid upon a polymer as the latter becomes extended (Hinch 1977; Rallison & Hinch 1988) – in order to determine to what extent gradients in shear can produce more pronounced variations in the conformation-average diffusivity, thereby leading to stronger migration effects.

REFERENCES

Agarwal, U. S., Dutta, A. & Mashelkar, R. A. 1994 Migration of macromolecules under flow: the physical origin and engineering implications. (Review article no. 45) *Chem. Engng Sci.* **49**, 1693–1717.

Aubert, J. H., Prager, S. & Tirrell, M. 1980 Macromolecules in nonhomogeneous velocity gradient fields. II. *J. Chem. Phys.* **73**, 4103–4112.

Aubert, J. H. & Tirrell, M. 1980 Macromolecules in nonhomogeneous velocity gradient fields. *J. Chem. Phys.* **72**, 2694–2701.

Batchelor, G. K. 1976 Brownian diffusion of particles with hydrodynamic interaction. *J. Fluid Mech.* **74**, 1–29.

Batchelor, G. K. 1977 Developments in microhydrodynamics. In *Theoretical and Applied Mechanics* (ed. W. T. Koiter), pp. 33–55. North Holland.

Bhave, A. V., Armstrong, R. C. & Brown, R. A. 1991 Kinetic theory and rheology of dilute, nonhomogeneous polymer solutions. *J. Chem. Phys.* **95**, 2988–3000.

Bird, R. B. 1979 Use of simple molecular models in the study of the mechanical behaviour of solutions of flexible macromolecules. *J. Non-Newtonian Fluid Mech.* **5**, 1–12.

Bird, R. B. & Warner, H. R., Jr. 1971 Hydrodynamic interaction effects in rigid dumbbell suspensions. I. Kinetic theory. *Trans. Soc. Rheol.* **15**, 741–750.

Brunn, P. O. 1983 Hydrodynamically induced cross stream migration of dissolved macromolecules (modelled as nonlinearly elastic dumbbells). *Intl J. Multiphase Flow* **9**, 187–202.

Brunn, P. O. 1987 Diffusion in concentrated polymer solutions: encapsulated FENE dumbbell model results. *J. Polymer Sci.* B *Polymer Phys.* **25**, 2085–2093.

Brunn, P. O. & Chi, S. 1984 Macromolecules in nonhomogeneous flow fields: a general study for dumbbell model macromolecules. *Rheol. Acta* **23**, 163–171.

Brunn, P. O. & Kaloni, P. N. 1985 Concentrated polymer solutions: non-uniform concentration profiles in tube flow. *J. Chem. Phys.* **83**, 2497–2503.

Cohen, Y. & Metzner, A. B. 1982 Slip phenomena in polymeric solutions flowing through small channels. *AIChE Symp. Ser.*, No. 212, **78**, 77–85.

Dongarra, J. J., Bunch, J. R., Moler, C. B. & Stewart, G. W. 1979 *LINPACK Users' Guide*. Philadelphia: SIAM.

EINSTEIN, A. 1956 *Investigations on the Theory of the Brownian Movement*. Dover.

GRASSIA, P. S., HINCH, E. J. & NITSCHE, L. C. 1995 Computer simulations of Brownian motion of complex systems. *J. Fluid Mech.* **282**, 373–403.

HAPPEL, J. & BRENNER, H. 1983 *Low Reynolds Number Hydrodynamics*. Martinus Nijhoff.

HINCH, E. J. 1977 Mechanical models of dilute polymer solutions in strong flows. *Phys. Fluids* **20**, S22–S30.

HINCH, E. J. & LEAL, L. G. 1971 The effect of weak Brownian rotations on particles in shear flow. *J. Fluid Mech.* **46**, 685–703.

HINCH, E. J. & LEAL, L. G. 1972 The effect of Brownian motion on the rheological properties of a suspension of non-spherical particles. *J. Fluid Mech.* **52**, 683–712.

JHON, M. S., SEKHON, G. & ARMSTRONG, R. 1987 The response of polymer molecules in a flow. *Adv. Chem. Phys.* **66**, 153–211.

LARSON, R. G. 1992 Flow-induced mixing, demixing, and phase transitions in polymeric fluids. *Rheol. Acta* **31**, 497–520.

LAYEC, Y. 1972 Contribution à l'étude numérique de la viscosité intrinsèque non-newtonienne de solutions d'ellipsoëdes rigides et application expérimental au poly-L-glutanmate de benzyle. Dissertation, Universite Louis Pasteur Strasbourg, September 13.

LEAL, L. G. & HINCH, E. J. 1971 The effect of weak Brownian rotations on particles in shear flow. *J. Fluid Mech.* **46**, 685–703.

MARRUCCI, G. 1972 The free energy constitutive equation for polymer solutions from the dumbbell model. *Trans. Soc. Rheol.* **16**, 321–330.

NITSCHE, J. M. & BRENNER, H. 1990 On the formulation of boundary conditions for rigid nonspherical Brownian particles near solid walls: applications to orientation-specific reactions with immobilized enzymes. *J. Colloid Interface Sci.* **138**, 21–41.

NITSCHE, J. M. & ROY, P. 1996 On the shear-induced alignment of nonspherical Brownian particles near walls. *AIChE J.* to appear.

ÖTTINGER, H. C. 1987 Consistently averaged hydrodynamic interaction for Rouse dumbbells: translational diffusivity. *J. Chem. Phys.* **87**, 6185–6190.

ÖTTINGER, H. C. 1989*a* Gaussian approximation for Hookean dumbbells with hydrodynamic interaction: translational diffusivity. *Colloid Polymer Sci.* **267**, 1–8.

ÖTTINGER, H. C. 1989*b* Diffusivity of polymers in dilute solutions undergoing homogeneous flows. *AIChE J.* **35**, 279–286.

PRAKASH, J. R. & MASHELKAR, R. A. 1991 The diffusion tensor for a flowing dilute solution of Hookean dumbbells: anisotropy and flow rate dependence. *J. Chem. Phys.* **95**, 3743–3748.

PRAKASH, J. R. & MASHELKAR, R. A. 1992 The diffusion tensor for Hookean dumbbells in steady shear flow: analytical approximation. *J. Rheol.* **36**, 789–805.

RALLISON, J. M. & LEAL, L. G. 1981 Dynamic light scattering from macromolecules: the separation of translation from rotational and deformational modes. *J. Chem. Phys.* **74**, 4819–4825.

SCHIEK, R. L. & SHAQFEH, E. S. G. 1995 A nonlocal theory for stress in bound, Brownian suspensions of slender, rigid fibres. *J. Fluid Mech.* **296**, 271–324.

SCHIEK, R. L. & SHAQFEH, E. S. G. 1997 Cross streamline migration of slender, Brownian fibres in plane Poiseuille flow. *J. Fluid Mech.* **332**, 23–39.

SEKHON, G., ARMSTRONG, R. C. & JHON, M. S. 1982 The origin of polymer migration in a nonhomogeneous flow field. *J. Polymer Sci. Polymer Phys. Ed.* **20**, 947–952.

SHAFER, R. H., LAIKEN, N. & ZIMM, B. H. 1974 Radial migration of DNA molecules in cylindrical flow. I. Theory of the free-draining model. *Biophys. Chem.* **2**, 180–184.

STASIAK, W. & COHEN, C. 1983 Dilute solutions of macromolecules in a rectilinear Poiseuille flow. *J. Chem. Phys.* **78**, 553–559.

STEWART, W. E. & SORENSEN, J. P. 1972 Hydrodynamic interaction effects in rigid dumbbell suspensions. II. Computations for steady shear flow. *Trans. Soc. Rheol.* **16**, 1–13.

TIRRELL, M. & MALONE, M. F. 1977 Stress-induced diffusion of macromolecules. *J. Polymer Sci. Polymer Phys. Ed.* **15**, 1569–1583.